Photoluminescence and Raman Scattering in Ag-doped ZnO Nanoparticles

R. Sánchez Zeferino, M. Barboza Flores, and U. Pal

Citation: Journal of Applied Physics **109**, 014308 (2011); doi: 10.1063/1.3530631
View online: http://dx.doi.org/10.1063/1.3530631
View Table of Contents: http://scitation.aip.org/content/aip/journal/jap/109/1?ver=pdfcov
Published by the AIP Publishing

Photoluminescence and Raman Scattering in Ag-doped ZnO Nanoparticles

R. Sánchez Zeferino,[1] M. Barboza Flores,[2] and U. Pal[1,a)]
[1]*Instituto de Física, Universidad Autónoma de Puebla, Apdo. Postal J-48, Puebla 72570, Mexico*
[2]*Centro de Investigación en Física, Universidad de Sonora, Apdo. Postal 5-088, Hermosillo, Sonora 83190, Mexico*

(Received 23 September 2010; accepted 17 November 2010; published online 7 January 2011)

Effects of Ag doping on the crystallinity and optical properties of zinc oxide (ZnO) nanoparticles have been studied by x-ray diffraction, diffuse reflectance spectroscopy, micro-Raman, and photoluminescence spectroscopy. It has been observed that while Ag-doping at low concentration improves the optoelectronic properties of ZnO nanostructures, Ag-doping at high concentrations drastically modify the emission behavior and lattice vibrational characteristics of the nanostructures. High Ag content in ZnO nanostructures causes lattice deformation, induces silent vibrational modes in Raman spectra, and reduces excitonic UV emission due to concentration quenching. © *2011 American Institute of Physics*. [doi:10.1063/1.3530631]

I. INTRODUCTION

Nanostructured semiconductors are of great interest due to their extraordinary physicochemical properties, which differ from their bulk counterparts. Zinc oxide (ZnO) is a II–VI compound semiconductor, promising for applications as gas sensors, piezoelectric transducers, and solar cell windows.[1,2] It has also been used for applications in optoelectronics, e.g., short wavelength light emitting diode, photodetector, ultraviolet (UV) laser, etc., due to its wide band gap (3.36 eV at room temperature) and large excitonic binding energy (60 meV).[3]

Fabrication of efficient devices based on semiconductor nanostructures requires in-depth understanding of their optoelectronic behaviors, which depend on their shape, size, and impurity contents. Recently, several research groups have reported that the doping process can influence the luminescence properties of ZnO; frequently leading to blueshift or redshift in its near band edge (NBE) emission and drastic changes in their visible emission.[4,5] On the other hand, luminescence properties of those nanostructures might also depend on their morphology, growth technique, synthesis conditions, and imperfections. For example, silver (Ag) doping has been seen to affect the photocatalytic activity of semiconductor nanostructures.[6] Role of Ag as a prominent luminescent activator in compound semiconductor has been reported by Park *et al.*[7]

Due to the vast optoelectronic applications of ZnO nanostructures, several theoretical and experimental studies have been made on the optical properties of ZnO nanostructures with different morphologies, such as nanoparticles, nanowires, nanobelts,[8] nanoprisms,[9] and nanostructured thin films.[10] Very often, two emission bands appear in the photoluminescence (PL) spectra of ZnO. One UV band located at about 3.23 eV, commonly attributed to its excitonic transition, and a broad yellow-green emission in between 2.33 and 2.48 eV, associated with defect states like oxygen vacancies (V_o) and interstitial zinc atoms (Zn_i).[11] While the origin of UV emission in ZnO is relatively well known, origin of the visible emissions is still considered controversial. It has been reported that both the UV and visible emission in ZnO can be tailored through metal doping.[12,13]

In the present article, we report on the synthesis of undoped and Ag-doped ZnO nanoparticles of the order of 100 nm diameters through nonionic polymer assisted thermolysis. Effects of Ag doping on the PL and Raman scattering behavior of the nanoparticles are studied in details.

II. EXPERIMENTAL

The procedure for preparing undoped and Ag-doped ZnO nanoparticles was as follows. First, a 20 ml aqueous solution (0.02 M) of zinc acetate dihydrate [$Zn(CH_3COO)_2 \cdot 2H_2O$, Baker, 99.9%] was prepared under mild magnetic stirring. After stirring this solution for about 20 min, 5.8 ml of polyethylene glycol-p-isocooctylphenyl ether, commonly known as Triton X100 [$(C_2H_4O)_nC_{14}H_{22}O$, Aldrich] was slowly added. For Ag doping, different amounts (nominally 0.5, 1.0, and 2.0 mol %) of silver nitrate [$AgNO_3$, Aldrich, 99.8%] were added to this mixture. The final solution was heated in a muffle furnace for 48 h at 260 °C (with 2 °C/min temperature increase). Finally, the resulting powder was air annealed in a 100 cm long horizontal (50 mm diameter) quartz tube furnace at 550 °C for 2 h.

The morphology and size of the nanoparticles were verified by a scanning electronic microscope (SEM, JEOL JSM-5600LV). Crystallinity of the nanostructures was analyzed using the Cu K_α radiation ($\lambda = 1.5406$ Å) of a Rigaku® x-ray diffractometer (XRD). Optical properties of the synthesized nanoparticles were studied by diffuse reflectance spectroscopy (DRS, Varian Cary 100 UV-Vis spectrophotometer with DRA-CA-30I diffuse reflectance accessory), micro-Raman spectroscopy (Horiba JOBIN-YVON spectrophotometer) and PL spectroscopy at different temperatures. For recording the PL spectra of the samples, a 0.5 m long Science Tech monochromator, a Hamamatsu photomultiplier, and a Janis cryogenic cooling system were used. The samples were excited with the 325 nm emission of a He–Cd laser.

a)Electronic mail: upal@sirio.ifuap.buap.mx.

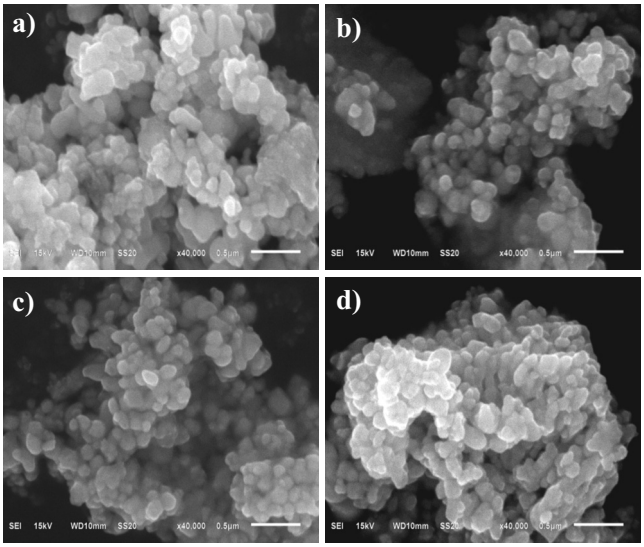

FIG. 1. Typical SEM micrographs of the (a) undoped, (b) 0.5%, (c) 1.0%, and (d) 2.0% Ag-doped ZnO nanostructures.

III. RESULTS AND DISCUSSION

Figure 1 shows the typical SEM micrographs of the ZnO nanoparticles prepared with different nominal concentrations of silver nitrate. Formation of quasisphreical ZnO particles in the 100–200 nm size range is clear from the micrographs. No appreciable change either in morphology or in size of the ZnO particles could be observed on Ag-doping [Figs. 1(b)–1(d)]. As can be seen from their XRD patterns (Fig. 2), all the samples were well crystalline, and of hexagonal wurtzite phase (JCPDS file no. 36-1451). However, the Ag-doped samples revealed some additional diffraction peaks (marked with " *") associated with the face-centered-cubic (fcc) phase of metallic Ag (JCPDS file no. 04-0783). In general, the intensity of the diffraction peaks associated with ZnO decreases and their full width at half maximum (FWHM) increases on Ag incorporation (see Table I), indicating a decrease in crystallinity of the nanostructures. While the decrease of crystallinity and a shift in position of the main diffraction peaks (Table I) indicate the incorporation of

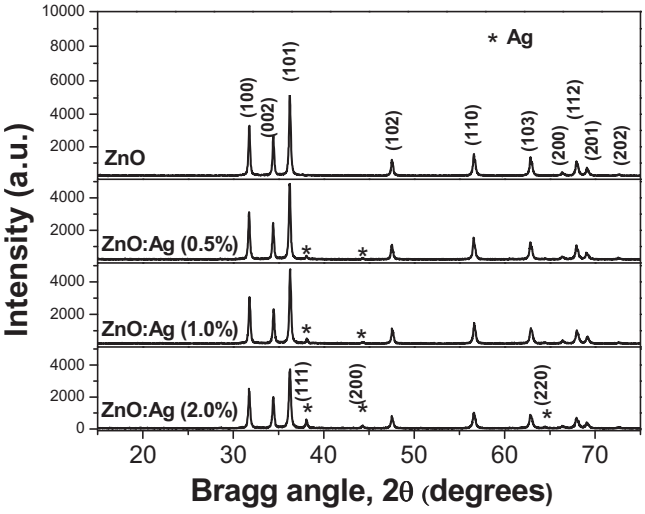

FIG. 2. XRD patterns of the undoped and Ag-doped ZnO nanoparticles.

TABLE I. Position, FWHM of the main diffraction peaks, along with the lattice parameter values calculated from the XRD patterns of the undoped and Ag-doped ZnO nanoparticles.

Nominal Ag concentration (at. %)	Position of the (101) diffraction peak and its FWHM (deg)	Position of the (002) diffraction peak and its FWHM (deg)	Lattice parameters (Å)	
			a	c
0	36.23 (0.22)	34.41 (0.19)	3.254	5.212
0.5	36.25 (0.22)	34.40 (0.20)	3.251	5.212
1.0	36.30 (0.23)	34.45 (0.20)	3.247	5.206
2.0	36.28 (0.25)	34.42 (0.21)	3.248	5.210

Ag^+ ions in the ZnO lattice sites, probably substituting Zn^{2+} ions, appearance of Ag peaks in the diffraction patterns indicates clearly the formation of crystalline silver clusters in the nanoparticles. It is worth mentioning that Ag^+ ions in ZnO lattice behave similar to other monovalent dopant ions like Na^+ and K^+, which have ability to occupy both the lattice and interstitial sites.[14] Limited incorporation of Ag^+ ions into the ZnO lattice through substitution of Zn^{2+} ions was due to their higher ionic radius (1.22 Å) in comparison with the radius of Zn^{2+} ions (0.74 Å).

Though the position of the NBE emission of ZnO could be blueshifted for its nanoparticles of diameters comparable or smaller than its excitonic diameter (7.4 nm) due to quantum size effect,[15] doping with appropriate element might cause both blue and redshifts. As the sizes of our undoped and Ag-doped ZnO particles were bigger than 100 nm, a quantum size effect is not expected to be observed, and any change in the band gap energy (E_g) could be attributed solely to Ag doping.

Diffuse reflectance spectra of all the samples (Fig. 3) revealed characteristic absorption edge near 380 nm. Undoped ZnO powders revealed high reflectance (~50%) in the visible region. Reflectance of the Ag-doped ZnO samples decreased with the increase in Ag concentration. Band gap energy of the samples was estimated through the Kubelka–Munk treatment to their DRS spectra, following the method reported earlier.[16] Figure 4 presents the Kubelka–Munk plots for the undoped and Ag-doped samples, used to determine their band gap energies. It can be observed that while the

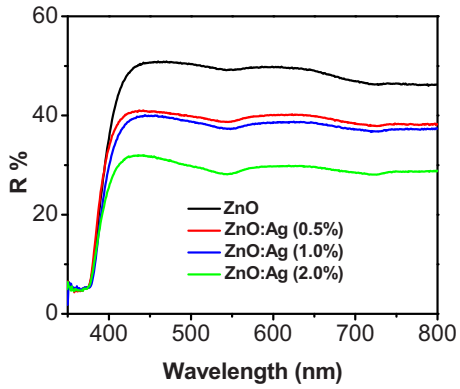

FIG. 3. (Color online) Diffuse reflectance spectra of the undoped and Ag-doped ZnO nanoparticles.

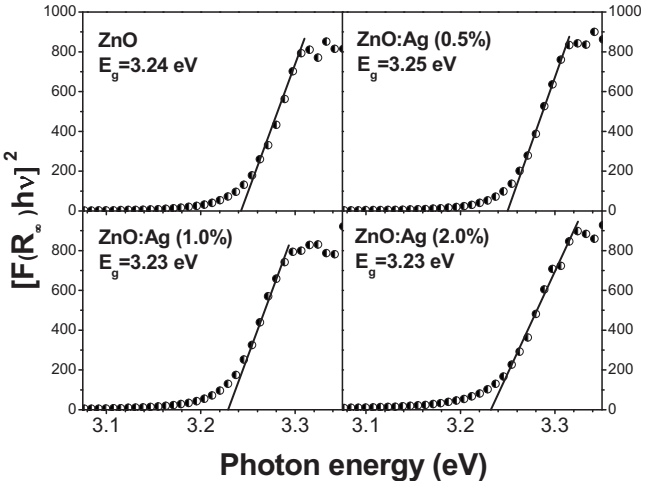

FIG. 4. Kubelka–Munk plots and band gap energy estimation for the undoped and Ag-doped ZnO nanoparticles.

band gap energy value for the sample doped with 0.5% (nominal) Ag did not change with respect to the undoped one, there occurred a small redshift (0.02 eV) for the samples doped with 1.0% and 2.0% Ag. Wang *et al.*[17] have observed a similar effect in their $Zn_{1-x}Cd_xO$ nanorods and nanoneedles due to Cd substitution in ZnO lattice. Kukreja *et al.*[18] also have reported a band gap energy value as low as 2.90 eV for the alloy made of ZnO and CdO.

In order to investigate the influence of Ag doping on the Raman scattering of ZnO nanoparticles, room temperature Raman spectra of all samples were measured. It is well known that wurtzite ZnO has eight sets of characteristic optical phonon modes at the center of Brillouin zone (Γ point),

$$\Gamma = 1A_1 + 2B_1 + 1E_1 + 2E_2, \quad (1)$$

where A_1 and E_1 are the two polar branches, which split into longitudinal optical (LO) and transversal optical components with different frequencies due to macroscopic electric fields associated with the LO phonons. The E_2 modes are nonpolar with low frequency mode (E_{2L}) associated to the heavy Zn sublattice and high frequency mode (E_{2H}) involving only oxygen atoms.[19] While the A_1, E_1, and E_2 modes are active in Raman and infrared spectra, the B_1 modes are generally inactive in Raman spectra and are so-called silent modes.

Figure 5 presents the room temperature Raman spectrum

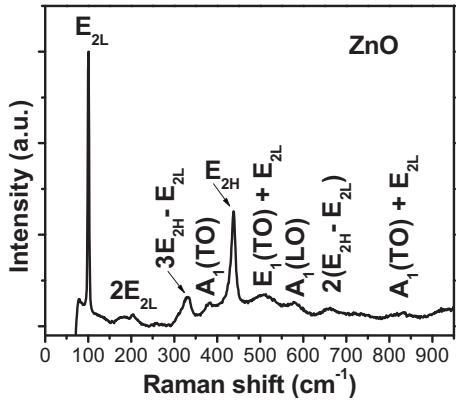

FIG. 5. Typical Raman spectrum of ZnO nanoparticles.

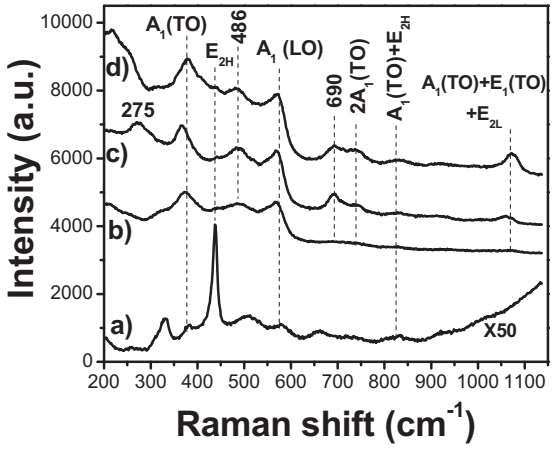

FIG. 6. Raman spectra of the ZnO nanoparticles containing: (a) 0%, (b) 0.5%, (c) 1.0%, and (d) 2.0% (nominal) of Ag.

of the undoped ZnO sample in the 50–800 cm^{-1} spectral range. The spectrum consists of four peaks located at about 100, 380, 437, and 580 cm^{-1}, which correspond to the E_{2L}, $A_1(TO)$, E_{2H}, and $A_1(LO)$ fundamental phonon modes of hexagonal ZnO, respectively. The Raman peak located at about 204 cm^{-1} was assigned to the $2E_{2L}$ second-order phonon mode. Other four Raman peaks located at about 331, 508, 664, and 822 cm^{-1} could be assigned to the $3E_{2H}-E_{2L}$, $E_1(TO)+E_{2L}$, $2(E_{2H}-E_{2L})$, and $A_1(TO)+E_{2L}$ multiphonon scattering modes, respectively.

Raman spectra of the Ag-doped ZnO nanoparticles with different Ag contents are shown in Fig. 6. The $A_1(TO)$ and $A_1(LO)$ polar branches appeared at about 380 cm^{-1} and 570 cm^{-1}, respectively, for all the samples. On incorporating Ag in ZnO, the $A_1(LO)$ peak broadened and shifted about 9 cm^{-1} toward lower energy. Such a shift and broadening in the $A_1(LO)$ phonon mode can be attributed to the scattering contributions of the $A_1(LO)$ branch outside the Brillouin zone center.[20] The $A_1(LO)$ phonon mode is commonly assigned to the oxygen vacancies,[21,22] zinc interstitials,[23,24] or defect complexes containing oxygen vacancy and zinc interstitial in ZnO.[23] Additionally, there appeared a broad Raman peak at about 486 cm^{-1} exclusively for the Ag-doped samples, which was assigned as the interfacial surface phonon mode in the literature.[25] This phonon mode cannot be a local vibrational mode associated to Ag ions as it was also observed for ZnO doped with Mn (Ref. 26) and Co.[27] The Raman peak appeared at about 690 cm^{-1} has also been reported for Co-doped ZnO.[28] However, its origin is not yet clear. The E_{2H} mode of ZnO appeared at about 437 cm^{-1} for the undoped sample. The intensity of this peak decreased drastically on increasing the silver concentration in the samples. We can recall that the incorporation of Ag in our ZnO nanoparticles reduces their crystallinity (Fig. 2); and such a drastic reduction in intensity of the E_{2H} mode might be due to the breakdown of translational crystal symmetry by the incorporated defects and impurity. Raman peaks appeared at about 754 and 1065 cm^{-1} could be assigned to the $2A_1(TO)$ second-order polar mode and multi-phonon mode, respectively. Intensity of these Raman peaks increased with the increase of Ag content.

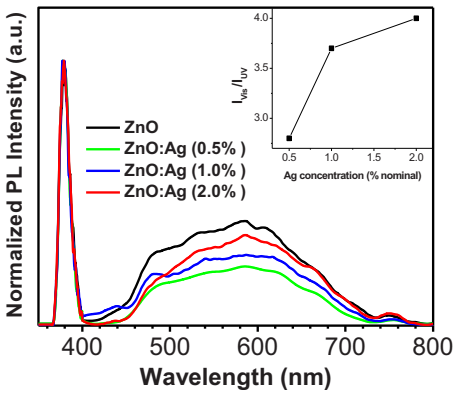

FIG. 7. (Color online) Room temperature PL spectra of the ZnO and Ag-doped ZnO nanoparticles. The inset shows the variation in relative intensity (I_{Vis}/I_{UV}) with Ag content in the samples.

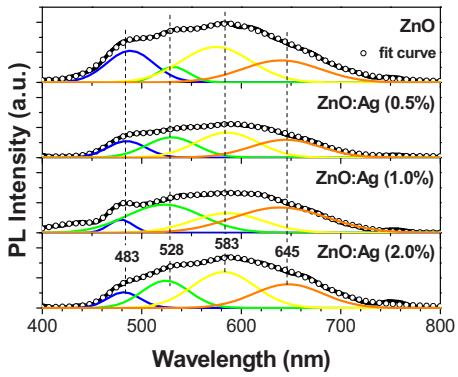

FIG. 8. (Color online) Gaussian deconvolution of the visible PL band for the ZnO nanoparticles containing: (a) 0%, (b) 0.5%, (c) 1.0%, and (d) 2.0% (nominal) of Ag.

For the case of ZnO:Ag (0.5%) sample, there appeared a Raman peak at about 275 cm^{-1} [Fig. 6(c)], which has also been reported for ZnO doped with Fe, Sb, Al, and Ga.[29] This anomalous vibrational mode could be associated to the lattice-host intrinsic defects created by doping, as it has also been observed for the ZnO samples doped with so many other elements. Several authors have assigned this anomalous mode to the B_1(low) silent mode due to its closeness to the position of theoretically calculated B_1 mode (261 cm^{-1}).[30]

Room temperature PL spectra of the undoped and Ag-doped ZnO nanostructures are presented in Fig. 7. There appeared an intense narrow emission band in the UV spectral range centered at around 380 nm for all the samples. Generally, this emission has been assigned to the free excitonic recombination in ZnO.[31] No appreciable change in the position of this UV band has been observed on silver doping. Apart from this UV band, there appeared another wider emission band in the visible spectral range, centered at around 580 nm. This multicomponent visible emission in ZnO has been frequently assigned to several intrinsic and extrinsic defects. As can be seen in the Fig. 7, the intensity of this visible emission initially decreases for 0.5% (nominal) silver doping, and then increases for higher Ag concentrations. Such anomalous intensity variation in Ag-doped ZnO nanostructures can be understood considering the Ag incorporation process in the nanoparticles. The Ag^{+} ions can be incorporated in to the ZnO nanostructures in two different ways: substituting Zn^{+2} ions creating doubly ionized oxygen vacancies ($V_O^{\cdot\cdot}$), or incorporating as interstitials (Ag_i).[32] While for low doping concentrations (e.g., 0.5%), most of the Ag^{+} ions might have been incorporated into the ZnO lattice through substitution, for higher concentrations, the excess amount of Ag^{+} ions incorporated in to the nanoparticles interstitially, creating larger amount of lattice defects. Presence of metallic Ag peaks in the XRD patterns of the Ag-doped samples supports our argument. From the (I_{Vis}/I_{UV}) intensity ratio plot against the silver concentration presented as the inset of the Fig. 7, it is very clear that a higher Ag concentration in the nanostructures incorporates higher amount of structural defects.

The broad visible emission band could be deconvoluted in to four Gaussian shaped components (Fig. 8) peaked around 583 nm (~2.12 eV), 483 nm (~2.56 eV), 528 nm (~2.35 eV), and 645 nm (~1.92 eV). While the component band close to 2.58 eV has been frequently designated as the blue emission[33,34] and associated to the intrinsic defects (vacancies or interstitials of O and Zn and their complexes) in ZnO nanostructures,[35] the component band at about 2.35 eV was assigned as the green emission and associated to the oxygen and zinc vacancies.[36,37] On the other hand, the component bands appeared at about 2.12 eV and 1.92 eV are frequently assigned as the yellow and orange emissions in ZnO, respectively, and associated with the excess oxygen (O_i) and interstitial zinc atoms (Zn_i).[38] As can be seen from the Fig. 8, while the intensity of the blue emission decreases, the intensity of the green emission increases with the increase in Ag concentration in the samples. While the incorporation of Ag does not affect the intensity of the orange emission considerably, the intensity of the yellow emission reduces up to 1.0% (nominal) of Ag, and then increases.

To determine the nature of the UV emission in our Ag-doped and undoped ZnO nanoparticles correctly, their room temperature PL spectra were recorded at different excitation intensities of the laser beam. Generally, the intensity of the NBE PL emission varies with the excitation power obeying the following relation:[39]

$$I = \beta P^{\alpha}, \tag{2}$$

where I is the PL intensity, β is a constant, P is the excitation power density, and α is an exponent. For the excitation energy exceeding the band gap energy, α varies in between 1 and 2 for excitonic transition, and $\alpha < 1$ for free to bound and donor-acceptor pair transitions.[40] In Fig. 9, the log-log plots of PL intensity as the function of excitation power are plotted for Ag-doped and undoped ZnO nanoparticles. As can be seen, the intensities of the UV emission under various excitation power densities could be fitted by the power law with superlinear dependence for all the samples, and the gradients of the plots (α) were 1.037, 1.090, 1.093, and 1.099 for the undoped, 0.5%, 1.0%, and 2.0% (nominal) Ag-doped ZnO nanostructures, respectively. These results indicate clearly an excitonic origin of the UV emission for all the samples; and the Ag doping does not alter the luminescence mechanism of ZnO nanoparticles.

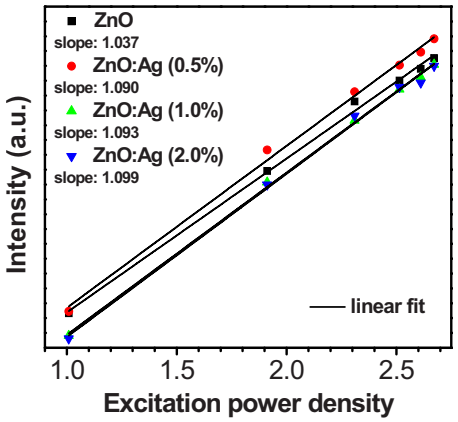

FIG. 9. (Color online) Log-log plots of PL intensity and excitation power for the Ag-doped and undoped ZnO nanoparticles.

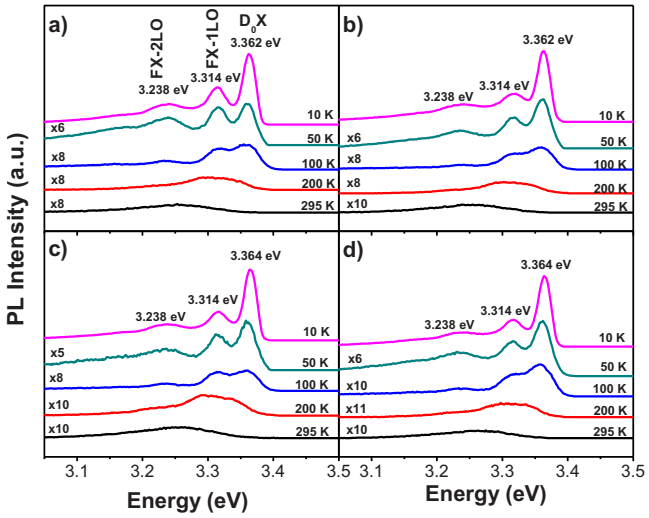

FIG. 10. (Color online) Low temperature (10 to 295 K) PL spectra of ZnO nanoparticles dopes with: (a) 0.0%, (b) 0.5%, and (c) 1.0% and 2.0% (nominal) Ag.

As can be observed from the Fig. 9, there is a significant increase in the UV emission intensity for the 0.5% Ag-doped sample in comparison with other samples, for the whole range of considered excitation power (2.3 to 0.05 mW). That indicates the efficiency of exciton recombination was high for this sample. However, the UV emission intensity decreased on increasing the Ag-content further. As has been stated earlier, for Ag-doping at lower concentrations (e.g., 0.5%), most of the incorporated Ag^+ ions occupy ZnO lattice through Zn^{2+} ion substitution. When the incident UV light (325 nm emission of the He-Cd laser beam) excites the carriers in ZnO nanostructures, the photocarriers can escape more easily from Ag ions than from the Zn ions, leading a quicker diffusion of excitons in ZnO. On the other hand, the probability of excitonic recombination would be high in Ag-doped ZnO nanoparticles due to increased exciton concentration.[41] For the samples with higher content of Ag^+ ions (e.g., ZnO prepared with 1.0%, and 2.0% of Ag), as a good fraction of Ag remain at interstitial sites of the ZnO lattice forming small silver clusters, they would act as recombination centers, reducing the effective concentration of free excitons (FXs) and hence the intensity of UV emission. This effect is commonly known as concentration quenching.

To study the origin of the UV emission in more detail, PL measurements for all the samples were carried out at different temperatures in between 10 and 295 K (Fig. 10).

There appeared three component peaks of the UV emission in the low-temperature PL spectra of the undoped and Ag-doped nanostructures. The predominant sharp peak appeared at about 3.362 eV could be assigned to a neutral donor bound exciton (D^0X).[42,43] On the other hand, the other two less intense peaks appeared at about 3.314 and 3.238 eV correspond to the LO phonon replicas of the FX recombination, assigned as FX-1LO and FX-2LO transitions. The observed energy separation between the two replicas was about 76 meV, which is consistent with the reported value (72 meV) for the LO phonon energy of ZnO.[44] The energy separation did not vary with the variation of Ag content in the nanostructures. However, the position of the D^0X transition slightly blueshifted (from 3.362 to 3.364 eV) for higher Ag contents (1.0% and 2.0%). Fang *et al.*[45] have also found a similar shift in the position of D^0X transition for their bent ZnO nanowires, and associated it to the compressive stains generated in the nanostructures due to bending. The small blueshift in the D^0X transition in our highly Ag-doped nanostructures could be associated to the compressive strain generated through Ag-doping, as has been observed from their XRD results (Table I). Generally a compressive strain causes a blueshift in PL, and tensile strain causes a redshift.[45]

On increasing the temperature, all the excitonic peaks moved toward lower energy and gradually became broader due to the LO-phonon scattering and increased thermal ionization of excitons.[46] Finally, above 200 K, all the excitonic emissions were quenched.

IV. CONCLUSIONS

Pure and Ag-doped ZnO nanoparticles of about 140 nm average size and relatively low size dispersion could be grown by nonionic polymer assisted thermolysis of zinc acetate. For a low concentration of doping, most of the incorporated silver ions occupy ZnO lattice sites through substitution of Zn ions, and for high Ag concentrations, most of the silver ions occupy interstitial sites forming small metallic clusters. While the incorporation of Ag in the ZnO nanostructures does not affect their band gap energy substantially, it affects their lattice vibration behaviors drastically. Accumulation of Ag at the interstitial sites causes a distortion in ZnO lattice, breaks down its translational symmetry, increasing the intensity of the $A_1(TO)$ and $A_1(LO)$ polar optical phonon modes. The lattice incorporated Ag ions increase the probability of excitonic transitions and hence the intensity of UV emission in the PL through an increase in the concentration of free excitonic states in the band structure of ZnO. On the other hand, the interstitial Ag atoms/ions produce lattice distortion, generate electron-phonon coupling, and reduce the intensity of UV emission, acting as PL quencher.

ACKNOWLEDGMENTS

The work was partially supported by VIEP-BUAP (Grant No. VIEP-EXC-2010-I3). R. Sánchez Zeferino acknowledges CONACyT, Mexico for granting the doctoral fellowship.

[1]T. C. Zhang, Z. X. Mei, Y. Guo, Q. K. Xue, and X. L. Du, J. Phys. D: Appl. Phys. **42**, 065303 (2009).
[2]Z. L. S. Seow, A. S. W. Wong, V. Thavasi, R. Jose, S. Ramakrishna, and G. W. Ho, Nanotechnology **20**, 045604 (2009).
[3]C. Klingshirn, Phys. Status Solidi B **71**, 547 (1975).
[4]X. B. Wang, C. Song, K. W. Geng, F. Zeng, and F. Pan, J. Phys. D: Appl. Phys. **39**, 4992 (2006).
[5]Z. F. Liu, F. K. Shan, J. Y. Sohn, S. C. Kim, G. Y. Kim, Y. X. Li, and Y. S. Yu, J. Electroceram. **13**, 183 (2004).
[6]R. H. Wang, J. H. Z. Xin, Y. Yang, H. F. Liu, L. M. Xu, and J. H. Hu, Appl. Surf. Sci. **227**, 312 (2004).
[7]W. Park, T. C. Jone, and C. J. Summers, Appl. Phys. Lett. **74**, 1785 (1999).
[8]X. Wang, Y. Ding, Z. Li, J. Song, and Z. L. Wang, J. Phys. Chem. C **113**, 1791 (2009).
[9]D. Wang and C. Song, J. Phys. Chem. B **109**, 12697 (2005).
[10]L. Zhao, J. Lian, Y. Liu, and Q. Jiang, Appl. Surf. Sci. **252**, 8451 (2006).
[11]S. H. Jeong, B. N. Park, S. B. Lee, and J. H. Boo, Surf. Coat. Technol. **193**, 340 (2005).
[12]S. Ananthakumar, S. Anas, J. Ambily, and R. V. Mangalaraja, J. Ceram. Proc. Res. **11**, 164 (2010).
[13]E. Monroy, F. Omnès, and F. Calle, Semicond. Sci. Technol. **18**, R33 (2003).
[14]J. Fan and R. Freer, J. Appl. Phys. **77**, 4795 (1995).
[15]H. S. Nalwa, *Encyclopedia of Nanoscience and Nanotechnology* (American Scientific Publishers, New York, 2004), Vol. 8, 336.
[16]A. Escobedo Morales, U. Pal, and M. Herrera Zaldivar, J. Nanosci. Nanotechnol. **8**, 6551 (2008).
[17]F. Wang, Z. Ye, D. Ma, L. Zhu, and F. Zhuge, J. Cryst. Growth **283**, 373 (2005).
[18]L. M. Kukreja, S. Barik, and P. Mishra, J. Cryst. Growth **268**, 531 (2004).
[19]C. X. Xu, X. W. Sun, X. H. Zhang, L. Ke, and S. J. Chu, Nanotechnology **15**, 856 (2004).
[20]M. Schumm, ZnO-based semiconductors studied by Raman spectroscopy: semimagnetic alloying, doping and nanostructures, Ph.D. thesis, Julius-Maximilians-Universität Würzburg, 2008.
[21]J. M. Liu, C. K. Ong, and L. C. Lim, Ferroelectrics **231**, 223 (1999).
[22]G. J. Exarhos and S. K. Sharma, Thin Solid Films **270**, 27 (1995).
[23]C. J. Youn, T. S. Jeong, M. S. Han, and J. H. Kim, J. Cryst. Growth **261**, 526 (2004).
[24]M. Tzolov, N. Tzenov, D. Dimova-Malinovska, M. Kalitzova, C. Pizzuto, G. Vitali, G. Zollo, and I. Ivanov, Thin Solid Films **379**, 28 (2000).
[25]B. Jusserand and M. Cardona, *Light Scattering in Solids V*, Topics in Applied Physics, edited by M. Cardona and G. Güntherodt (Springer, Heidelberg, 1989), Vol. 66, p. 48.
[26]C. Vargas-Hernández, F. N. Jiménez-García, and J. F. Jurado, Rev. LatinAm. Metal. Mater. **S1**, 501 (2009).
[27]H. Zhou, L. Chen, V. Malik, C. Knies, D. M. Hofmann, K. P. Bhatti, S. Chaudhary, P. J. Klar, W. Heimbrodt, C. Klingshirn, and H. Kalt, Phys. Status Solidi **204**, 112 (2007).
[28]N. Hasuike, R. Deguchi, H. Katoh, K. Kisoda, K. Nishio, T. Isshiki, and H. Harima, J. Phys.: Condens. Matter **19**, 365223 (2007).
[29]F. J. Manjón, B. Marí, J. Serrano, and A. H. Romero, J. Appl. Phys. **97**, 053516 (2005).
[30]J. Serrano, A. H. Romero, F. J. Manjón, R. Lauck, M. Cardona, and A. Rubio, Phys. Rev. B **69**, 094306 (2004).
[31]C. Ton-That, M. Foley, and M. R. Phillips, Nanotechnology **19**, 415606 (2008).
[32]S. T. Kuo, W. H. Tuan, J. Shieh, and S. F. Wang, J. Eur. Ceram. Soc. **27**, 4521 (2007).
[33]Z. Fu, B. Lin, G. Liao, and Z. Wu, J. Cryst. Growth **93**, 316 (2008).
[34]L. Dai, X. L. Chen, W. J. Wang, T. Zhou, and B. Q. Hu, J. Phys.: Condens. Matter **15**, 2221 (2003).
[35]R. Dingle, Phys. Rev. Lett. **23**, 579 (1969).
[36]B. Lin, Z. Fu, and Y.Jia, Appl. Phys. Lett. **79**, 943 (2001).
[37]Z. L. Wang, J. Phys.: Condens. Matter **16**, R829 (2004).
[38]N. O. Korsunska, L. V. Borkovska, B. M. Bulakh, L. Yu. Khomenkova, V. I. Kushnirenko, and I. V. Markevich, J. Lumin. **733**, 102 (2003).
[39]T. Schmidt, K. Lishka, and W. Zulehner, Phys. Rev. B **45**, 8989 (1992).
[40]Z. C. Feng, A. Mascarenhas, and W. J. Choyke, J. Lumin. **35**, 329 (1986).
[41]Y. Zhang, Z. Zhang, B. Lin, Z. Fu, and J. Xu, J. Phys. B **109**, 19200 (2005).
[42]W. W. Liu, B. Yao, Y. F. Li, B. H. Li, Z. Z. Zhang, C. X. Shan, D. X. Zhao, J. Y. Zhang, D. Z. Shen, and X. W. Fan, Thin Solid Films **518**, 3923 (2010).
[43]F. Fang, D. Zhao, B. Li, Z. Zhang, J. Zhang, and D. Shen, J. Phys. D: Appl. Phys. **42**, 135415 (2009).
[44]T. V. Butkhuzi, T. G. Chelidze, A. N. Georgobiani, D. L. Jashiashvili, T. G. Khulordava, and B. E. Tsekvava, Phys. Rev. B **58**, 10692 (1998).
[45]F. Fang, D. Zhao, B. Li, Z. Zhang, D. Shen, and X. Wang, J. Phys. Chem. C **114**, 12477 (2010).
[46]T. Makino, C. H. Chia, N. T. Tuan, Y. Segawa, M. Kawassaki, A. Ohtomo, K. Tamura, and H. Koinuma, Appl. Phys. Lett. **76**, 3549 (2000).